Photoelectron Spectroscopic Studies of the Electronic Structure and Bonding in TiC and TiN

Stephen V. Didziulis,* Jeffrey R. Lince, and Thomas B. Stewart

Surface Science Department, Mechanics and Materials Technology Center, The Aerospace Corporation, El Segundo, California 90245

Elliot A. Eklund

IBM T. J. Watson Research Center, P.O. Box 218, Yorktown Heights, New York 10598

*Received October 6, 1993**

Titanium carbide (TiC) and titanium nitride (TiN) possess remarkable physical properties, such as extremely high hardness and melting point, that promote their use as antiwear materials under harsh tribological conditions. These physical properties must arise from chemical bonding phenomena that result from the inclusion of the non-metal atom within the metallic matrix, and these bonding phenomena should be apparent in measurements of the valence-band electronic structures of TiC and TiN. This paper explores the surface electronic structure and bonding in TiC(100) and TiN(110) with core and valence level photoelectron spectroscopies (PES's) using X-rays (1486.6 eV) and synchrotron radiation in the range 28–180 eV. Intensity changes in the valence-band features are followed as a function of incident photon energy; these changes are then compared to theoretical atomic photoionization cross sections to determine the atomic origins of these features. Resonant PES at the Ti 3p absorption edge is used to determine titanium 3d contributions to the valence band and to show differences in the electronic structures in TiC and TiN. A new resonance phenomenon near the Ti 3s edge in TiC was observed, and its possible assignment is discussed. The electronic structure and bonding in these materials is well described by molecular orbital theory, where the Ti and non-metal ions in their formal oxidation states (e.g., Ti^{4+} and C^{4-} in TiC) undergo covalent bonding interactions. Overall, the PES results indicate greater covalent mixing for TiC as compared to TiN, consistent with the differences in the electronegativities of the atoms. Specifically, stronger covalent interactions between the C 2s, 2p and the Ti 3d, 4s, 4p levels must occur to explain the spectroscopic differences between TiC and TiN. In addition, there is no evidence for an occupied TiC valence level having predominantly Ti character (unlike TiN), precluding the existence of direct Ti–Ti bonding in TiC. Any such orbital overlap is significantly affected by the carbon atoms in the lattice.

Introduction

Titanium carbide (TiC) and titanium nitride (TiN), along with other transition metal carbides and nitrides, have attracted a great deal of attention in several communities due to their remarkable physical properties. For example, TiN is currently widely used as a wear-resistant coating in the tool industry[1] and TiC coatings are being incorporated into ball bearings to enhance life and performance.[2] Both TiC and TiN are extremely hard, have very high melting points, and exhibit metallic-like electrical conductivity, as demonstrated in Table 1, while being significantly less reactive than most metals, especially titanium. Despite the intense interest in these materials, a fundamental understanding of the chemical bonding properties controlling their remarkable physical properties has not been reached. This paper details experimental investigations of the electronic structure and bonding properties of TiC and TiN using variable photon energy photoelectron spectroscopy (PES) and resonant photoelectron spectroscopy. A significant amount of work has been conducted on TiC and TiN in both experimental[6–16] and theoretical[15,17–24] electronic structure investigations. In general, these studies have focused more on the electronic-band structures of these extended-lattice, rock-salt materials with relatively little regard for understanding chemical bonding phenomena.[25,26] As such, the

Table 1. Selected Physical Properties of TiC and TiN Compared to Ti

material	hardness (kg/mm²)	mp (°C)	resistivity (μΩ cm)
Ti	200[3]	1600[4]	42[4]
TiC	3000[5]	3140[5]	200[4]
TiN	2000[5]	2930[5]	20[4]

* Abstract published in *Advance ACS Abstracts,* March 15, 1994.

(1) Cheng, H. S.; Chang, T. P.; Sproul, W. D. In *Mechanics of Coatings, Leeds-Lyon 16*; Dowson, D., Taylor, C. M., Godet, M., Eds.; Tribology Series 17; Elsevier Science Publishers B.V.: Amsterdam, 1990; pp 81–88.
(2) Boving, H. J.; Hintermann, H. E.; Stehle, G. *Lubr. Eng.* **1981,** *37,* 534.
(3) Tabor, D. *The Hardness of Metals*; Oxford University Press: London, 1951.
(4) Weast, R. C., Ed. *CRC Handbook of Chemistry and Physics,* 64th ed.; CRC Press: Boca Raton, FL, 1983.
(5) Toth, L. E. *Transition Metal Carbides and Nitrides*; Academic Press: New York, 1971.
(6) Ihara, H.; Kumashiro, Y.; Itoh, A. *Phys. Rev. B* **1975,** *12,* 5465.
(7) Hagström, A. L.; Johansson, L. I.; Jacobsson, B. E.; Hagström, S. B. M. *Solid State Commun.* **1976,** *19,* 647.
(8) Hagström, A. L.; Johansson, L. I.; Hagström, S. B. M. Christensen, A. N. *J. Electron. Spectrosc. Relat. Phenom.* **1977,** *11,* 75.
(9) Johansson, L. I.; Stefan, P. M.; Shek, M. L.; Christensen, A. N. *Phys. Rev. B* **1980,** *22,* 1032.
(10) Weaver, J. H.; Bradshaw, A. M. van der Veen, J. F.; Himpsel, F. J.; Eastman, D. E.; Politis, C. *Phys. Rev. B* **1980,** *22,* 4921.
(11) Oshima, C.; Aono, M.; Tanaka, T.; Kawai, S.; Zaima, S.; Shibata, Y. *Surf. Sci.* **1981,** *102,* 312.
(12) Zaima, S.; Shibata, Y.; Adachi, H.; Oshima, C.; Otani, S.; Aono, M.; Ishizawa, Y. *Surf. Sci.* **1985,** *157,* 380.
(13) Edamoto, K.; Anazawa, T.; Mochida, A.; Itakura, T.; Miyazaki, E.; Kato, H.; Otani, S. *Phys. Rev. B* **1992,** *46,* 4192.
(14) Johansson, L. I.; Callenas, A.; Stefan, P. M.; Christensen, A. N.; Schwarz, K. *Phys. Rev. B* **1981,** *24,* 1883.
(15) Bringans, R. D. Höchst, H. *Phys. Rev. B* **1983,** *30,* 5416.
(16) Lindberg, P. A. P.; Johansson, L. I.; Lindstrom, J. B.; Law, D. S. L. *Phys. Rev. B* **1987,** *36,* 939.
(17) Wimmer, E.; Neckel, A.; Freeman, A. J. *Phys. Rev. B* **1985,** *31,* 2370.
(18) Blaha, P.; Redinger, J.; Schwarz, K. *Phys. Rev. B* **1985,** *31,* 2316.
(19) Pai, V. A.; Sather, A. P.; Marathe, V. R. *J. Phys. Condens. Matter* **1990,** *2,* 9363.
(20) Ivanovskii, A. L.; Zhilyaev, V. A. *Phys. Status Solidi* **1991,** *168,* 9.
(21) Yip, K. L.; Kunz, A. B.; Williams, W. S. *Phys. Status Solidi* **1976,** *75,* 533.
(22) Gubanov, V. A.; Connolly, J. W. D. *Chem. Phys. Lett.* **1976,** *44,* 139.

0020-1669/94/1333-1979$04.50/0

extent of the participation of the non-metal atom in chemical bonding, the possibility of Ti–Ti bonding, and the relative contributions of ionic and covalent-bonding interactions for these materials that were historically termed "interstitial" compounds remain unclear.

Both TiC and TiN are fascinating materials from an inorganic chemistry point of view. The rock-salt structure forces the C and N atoms to adopt octahedral bonding environments that are unusual for first-row elements and cannot be described with valence-bond theory. The rock-salt structure also suggests the importance of Coulomb interactions because many ionic materials adopt this structure. Alternatively, the fact that the compounds are often substoichiometric with respect to the non-metal atom supports the interstitial compound description, where the C and N atoms simply fill octahedral voids in the metallic lattice. However, the lattice structure changes from hexagonal-closest-packed to face-centered-cubic upon forming the carbide (or nitride) from the metal, and the metal–metal distance increases by 0.16 Å (0.1 Å in the nitride), implying that significant bonding changes are occurring in the materials. Furthermore, neither an ionic nor an interstitial description of these materials can completely explain their tremendously high hardnesses, melting points, and electrical conductivities, all of which suggest a reliance on covalent bonding. The likely answer to this puzzle probably exists in a complex bonding scenario that relies on a combination of these bonding phenomena and results in the remarkable properties of these materials and other transition metal carbides and nitrides. An additional factor to be explored in a comparison of TiC and TiN bonding is the greater electronegativity of N that should result in more ionic interactions in TiN (and more covalent bonding in TiC).

This paper presents experimental results of electronic structure determinations using photoelectron spectroscopies. The majority of the results will focus on TiC, and comparisons will be drawn to similar results obtained on TiN. The goal of this work is to use the intensity changes observed with varying photon energy and resonant effects in PES to determine the atomic subshell contributions to the valence-band density of states. This will enable us to understand the valence-band electronic structure and shed light on the bonding phenomena giving rise to the physical properties cited above. Comparisons of the experimental work to ligand field–molecular orbital descriptions of the TiC and TiN electronic structure, which allow for covalent bonding interactions in ionic materials, will be made. In addition, this work should lead to an increased understanding of the surface chemical bonding and reactivity of these materials because the PES techniques are also quite surface sensitive. Finally, since our interest in these materials primarily concerns their tribological behavior, the implications of these results with regard to their friction and wear properties in mechanical systems will be explored.

Experimental Section

X-ray photoelectron spectroscopy (XPS) data were obtained with a Surface Science Instruments Model 301 X-probe spectrometer. The core and valence level data were obtained with a 300-μm-diameter spot from the monochromatized Al Kα source. The analyzer has a 30° cone of acceptance, with the central axis of the acceptance cone aligned 60° from the surface normal. The analyzer's pass energy was set at 50 eV. These parameters produce a $4f_{7/2}$ peak from clean gold foil at 84.0 eV, with a full-width-at-half-maximum of 0.95 eV. All binding energies reported in this paper are referenced to the spectrometer Fermi level. The spectrometer is housed in an ion- and titanium-sublimation-pumped vacuum system having a base pressure of $<1 \times 10^{-10}$ Torr that has been described in the literature.[27] Ion sputtering was performed with a Leybold-Heraeus IQE 12/38 ion gun in rastering mode. Low-energy electron diffraction (LEED) analyses were performed with Princeton Research Instruments Model RVL-8-120 reverse-view optics located in a separate sample prepartaion chamber having a base pressure of 1×10^{-10} Torr. Samples were transferred between the two chambers under ultrahigh-vacuum conditions.

The variable photon-energy valence-band and resonant PES data were obtained at the National Synchrotron Light Source, beam line U8B. This beam line uses two toroidal grating monochromators and has been described in detail in the literature.[28] The electron spectrometer used a high-resolution ellipsoidal mirror design that allowed the collection of angle-integrated PES data with a solid angle of approximately 2π sr. The collection angle was centered approximately normal to the surface. The spectrometer has been described in the literature.[29] The spectrometer is housed in an ion- and titanium-sublimation-pumped chamber having a base pressure of $<1 \times 10^{-10}$ Torr. The chamber is directly connected to a sample preparation chamber in which sample cleaning was performed. The preparation chamber has a base pressure of approximately 2×10^{-10} Torr. The intensity of the synchrotron radiation at a given photon energy was monitored by measuring the total current resulting from electron emission from the beam-line, gold-coated final focusing mirror. This signal was measured with an electrometer, and the data signals were divided by the flux channel. The resolution of the system (including both the monochromator and spectrometer) was estimated to be approximately 0.3–0.5 eV, depending on photon energy for collection of PES data. To obtain absorption edge data, constant final-state spectra (CFS) were obtained by collecting low-energy electrons (either 10 or 15 eV) from the secondary electron tail in a window 0.2 eV wide.

The TiC(100) sample was obtained as a gift from UBE Industries of Japan, and the growth techniques used are described in the literature.[30] The crystal grower's estimated stoichiometry of the material was $TiC_{0.9-0.92}$, although our quantitative XPS results showed the surface to have 1:1 stoichiometry (within the ±5% error of the technique). The crystal was polished with diamond paste down to 0.05-μm grit size and solvent-cleaned with ethanol and acetone. Sample cleaning in the vacuum chambers was performed in two different ways. For the XPS experiments, the sample was subjected to argon ion sputter/anneal cycles until the oxygen signal was minimized (<5 atom %). The accelerating potential of the Ar ion beam was decreased from 2 kV to 1.5, 1.0, and 0.5 kV, and the sample was bombarded while hot (650–700 °C); the sample was annealed at 650 °C following the sputter sequence. Low-energy electron diffraction of the clean surface showed the expected (100)-1×1 pattern after several treatments, and the C and Ti XPS core levels were narrow singlets, indicating limited surface damage after the sputter/anneal cycles. To obtain the synchrotron data, the sample was electron-beam-heated to approximately 1500 °C for 15–20 s. The Ti 3p core level was very sharp following the high-temperature flash, and no other valence-band peaks (particularly the O 2s), which would have indicated the presence of impurities, were observed in the data.

The TiN(110) sample was grown by reactive sputtering techniques on a MgO single crystal, following the methods of Johansson et al.[31] This crystal face was chosen for study rather than a (100) sample produced by the same methods because XPS studies showed the material to contain fewer C (≤2 atom %) and O (≤6 atom %) impurities. This sample was cleaned using similar sputter/anneal cycles as described above for TiC. We were unable to remove all impurities from this material, which was prepared in a diffusion-pumped deposition system having a base pressure of approximately 1×10^{-7} Torr. The Ti:N stoichiometry was 1:1 (within the experimental error of XPS), and core level XPS showed that no higher oxidation states of Ti were present (i.e., no TiO_2). Following sputter/anneal cycles, LEED patterns obtained on this surface indicated a square lattice with spot splitting that was possibly the result of surface faceting.

(23) Neckel, A.; Rastle, P.; Eibler, R.; Weinberger, P.; Schwartz, K. *J. Phys. C* **1976**, *9*, 579.
(24) Neckel, A. *Int. J. Quantum Chem.* **1983**, *23*, 1317.
(25) Wijeyesekera, S. D.; Hoffmann, R. *Organometallics* **1984**, *3*, 949.
(26) Jansen, S. A.; Hoffmann, R. *Surf. Sci.* **1988**, *197*, 474.
(27) Lince, J. R.; Didziulis, S. V.; Shuh, D. K.; Durbin, T. D.; Yarmoff, J. A. *Surf. Sci.* **1992**, *277*, 43.
(28) Himpsel, F. J.; Jugnet, Y.; Eastman, D. E.; Donelon, J. J.; Grimm, D.; Landgren, G.; Marx, A.; Morar, J. F.; Oden, C.; Pollock, R. A. *Nucl. Instrum. Methods* **1984**, *222*, 107.
(29) Eastman, D. E.; Donelon, J. J.; Hien, N. C.; Himpsel, F. J. *Nucl. Instrum. Methods* **1980**, *172*, 327.
(30) Otani, S.; Honma, S.; Tanaka, T.; Ishizawa, Y. *J. Cryst. Growth* **1983**, *61*, 1.
(31) Johansson, B. O.; Sundgren, J.-E.; Greene, J. E.; Rocket, A.; Barnett, S. A. *J. Vac. Sci. Technol. A* **1985**, *3*, 303.

Table 2. Core-Level Binding Energies (eV) for TiC and TiN

material	C (N) 1s	Ti $2p_{3/2}$	Ti 3p
TiC	281.6	454.7	33.8
TiN	397.2	455.1	34.2

Results and Analysis

A. Core Level PES. The core level binding energies obtained with both XPS and synchrotron PES are presented in Table 2. The C and N 1s levels in TiC and TiN both show a chemical shift to lower binding energy compared to "elemental" values (284.5 for the C 1s for graphite[32] and 399.3 for the N 1s in N_2H_4[33]), which is expected for these materials and has been observed before.[34,35] In the past, there was some controversy regarding the direction[36] and extent[37] of electron transfer in these materials, but these results are unambiguous; the Ti atom transfers charge to C (or N), consistent with the carbide and nitride labels placed on these materials. In addition, a comparison of the titanium core levels should provide an indication of the relative amount of charge transfer for the two materials. The binding energy of the Ti $2p_{3/2}$ core level in TiC was measured as 454.7 eV, while in TiN, this core level binding energy was measured as 455.1 eV. Both the Ti and non-metal core levels for each material are close (within ±0.2 eV) to literature values for near-stoichiometric TiC and TiN.[34,35] The Ti 2p levels in TiN also exhibit satellite peaks located approximately 2.5 eV to higher binding energy.[38] These satellites are generally attributed to shake-up relaxation phenomena.[39] (In ref 39, two shake-up final states are viewed as dominating this feature at energies 1.6 and 3.1 eV from the main peaks. Strydom and Hofmann claim that these transitions can be well described as Ti 3d → 3d shake-up final states.) For comparison, the $2p_{3/2}$ binding energy for elemental Ti is generally measured in the range 453.8–454.0 eV, while that of fully oxidized Ti in TiO_2 is 458.6 eV. In addition, the Ti 3p core levels were measured both in the XPS facility and with synchrotron radiation, and the binding energies were determined to be 33.8 eV for TiC and 34.2 eV for TiN. For comparison, the literature 3p binding energy for elemental Ti is 32.5 eV, and for TiO_2, it is 37.5 eV. These core level data indicate that the trend expected for TiC and TiN, based on atomic electronegativities, is observed; that is, more charge separation (and hence more ionic binding) occurs in TiN.

B. Variable Photon Energy PES of TiC. Figure 1 presents a PES valence band of TiC(100) obtained with 100-eV photons. This spectrum shows four distinct peaks, with binding energies of approximately 10.5, 6.0, 4.0, and 2.0 eV, along with a feature very close to the Fermi level (0.5 eV), labeled A–E, respectively. The shape of the spectrum is consistent with previously published angle-integrated TiC(100) data, but with generally higher resolution.[7,11]

The variation of the TiC valence-band spectrum with photon energy is presented in Figure 2. The data in Figure 2 were obtained at selected photon energies between 32 and 1486.6 eV to demonstrate how general changes in cross sections affect spectral intensities. The spectra have been normalized to the most intense feature, and the normalization factors for the synchrotron data (32–180 eV) are provided in the figure caption to allow comparison of absolute spectral intensities. In addition, the data presented in Figure 2 were selected to avoid photon energies where resonance

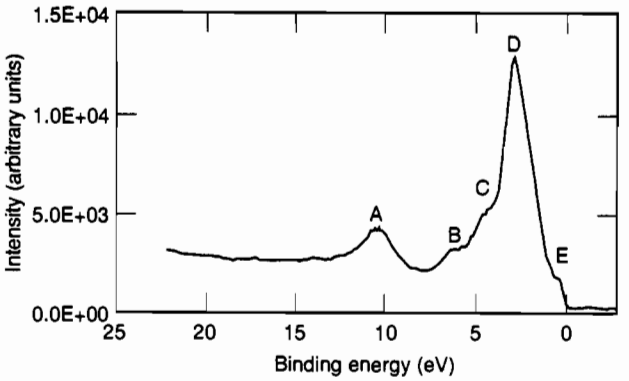

Figure 1. Valence-band photoelectron spectrum of TiC(100) obtained with 100-eV photons. The peaks are labeled as described in the text, and all binding energies are given relative to the Fermi level.

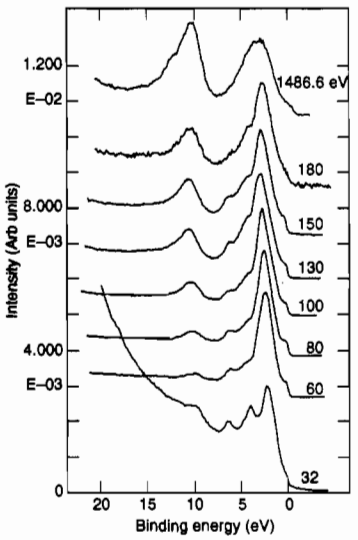

Figure 2. TiC(100) valence-band spectra obtained at the various photon energies listed on each spectrum. The 1486.6-eV data were obtained with a different spectrometer without photon-flux normalization. All data have been normalized to the most intense feature, and the normalization factors used for the synchrotron data were as follows: 32 eV, 1.4; 60 eV, 1; 80 eV, 1.2; 100 eV, 2.4; 130 eV, 10.5; 150 eV, 23.6; 180 eV, 62.2.

effects associated with Ti absorption edges are evident (particularly the 35–55-eV range near the Ti 3p edge). Resonant PES results will be presented and discussed in detail in following sections.

The most obvious change occurring from the very low- to high-energy data in Figure 2 is the increase in the relative intensity of the 10.5-eV peak (peak A) with increasing photon energy. This peak has been previously assigned as photoemission from the C 2s level, and a comparison to the theoretical atomic subshell photoionization cross sections[40] presented in Figure 3 certainly supports this assignment. In Figure 3A, the theoretical atomic subshell cross sections (normalized per electron) show the general trend of decreasing absolute intensity for all cross sections with increasing photon energy, but with less change for the C 2s level relative to the C 2p and Ti 3d, as demonstrated in the inset. This effect is more evident in Figure 3B, where the relative cross sections for the important atomic levels are plotted following normalization of the total valence cross section (i.e., the sum of the C 2s, C 2p, Ti 3d, and Ti 4s) to 1 at each photon energy. In the Figure 3B plot, the C 2s and Ti 4s cross sections gain relative intensity with increasing photon energy, the C 2p drops dramatically, and the Ti 3d has a relative intensity maximum near 80 eV.

The main valence-band features (peaks B–E) undergo more subtle intensity changes with increasing photon energy, and these

(32) Smith, K. L.; Black, K. M. *J. Vac. Sci. Technol., A* **1984**, *2*, 744.
(33) Biner, H.; Sellman, D. *Z. Naturforsch.* **1978**, *33B*, 173.
(34) Johansson, L. I.; Hagström, A. L.; Jacobson, B. E.; Hagström, S. B. M. *J. Electron Spectrosc. Relat. Phenom.* **1977**, *10*, 259.
(35) Burrow, B. J.; Morgan, A. E.; Ellwanger, R. C. *J. Vac. Sci. Technol., A* **1986**, *4*, 2463.
(36) Lye, R. G.; Logothetis, E. H. *Phys. Rev.* **1966**, *147*, 622.
(37) Ramqvist, L.; Hamrin, K.; Johansson, G.; Fahlman, A.; Nordling, C. *J. Phys. Chem. Solids* **1969**, *30*, 1835.
(38) Porte, L.; Roux, L.; Hanus, J. *Phys. Rev. B* **1983**, *28*, 2314.
(39) Strydom, I. leR.; Hofmann, S. *J. Electron. Spectrosc. Relat. Phenom.* **1991**, *56*, 85.
(40) Yeh, J. J.; Lindau, I. *At. Data Nucl. Data Tables* **1985**, *32*, 1.

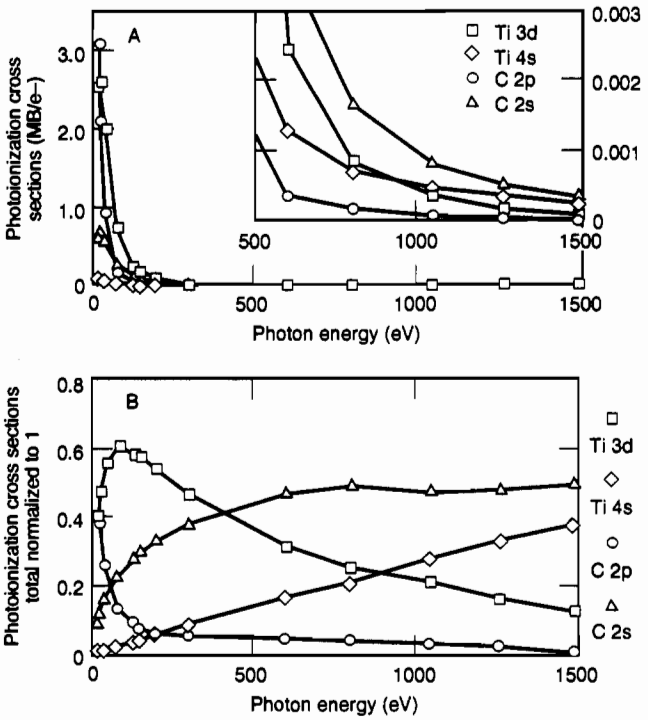

Figure 3. Plots of the theoretical atomic subshell photoionization cross sections for the important valence orbitals in TiC. (A) Absolute cross sections for the Ti 3d and 4s and the C 2s and 2p are levels provided normalized per electron. (B) Relative cross sections are provided by normalizing the total cross section at each photon energy to 1 and determining the contribution of each subshell normalized per electron.

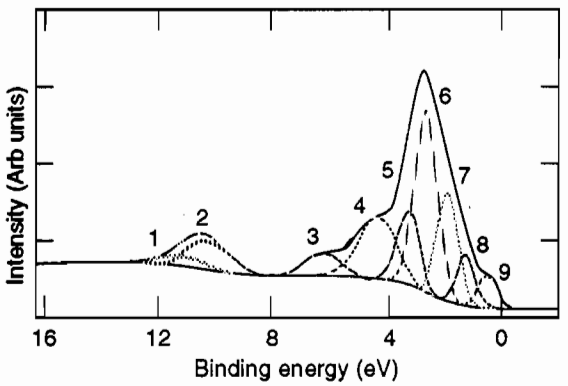

Figure 4. Fit of the TiC 100-eV spectrum using nine Gaussian peaks as labeled on the figure and provided in Table 3. Three Gaussians are used in the peak D region to account for asymmetries in this peak that became evident in the resonant PES data discussed in the text.

changes are best studied through fitting of the data with Gaussian peaks. Fits of the valence-band data shown in Figure 2 were performed using nine Gaussian peaks. The need for nine peaks is demonstrated in Figure 4, where two peaks were needed to fit the asymmetric C 2s region (peak A), one Gaussian each for peaks B and C, three Gaussians were used in the peak D region to account for asymmetries in this feature, and two Gaussians were used in the peak E region to fit the sharp drop off at the Fermi edge. The binding energies and widths of the Gaussians used in the fits are provided in Table 3. In the fitting process, the peak widths and energies were allowed to vary slightly (±0.2 eV) to account for changes in experimental resolution and background contributions to the data that accompany changes in incident photon energy. The spectral backgrounds must be taken into account for accurate fits, especially for the low-photon-energy data where the secondary electron tails has a large influence. For the Figure 2 data, Shirley backgrounds[41] were used in all fits. The 32-eV data were analyzed in three different

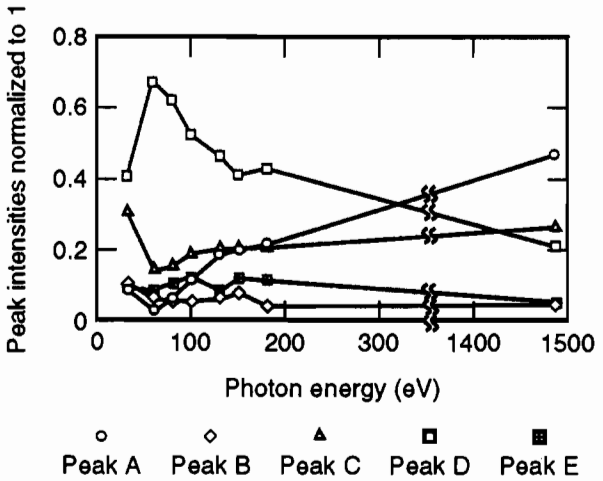

Figure 5. Experimental intensities for peaks A–E as determined by fits to the spectra in Figure 2. The peak intensities for this graph were determined by summing the Gaussians contributing to the five features that are clearly evident in the data. The total intensity at each photon energy has been normalized to 1 to allow comparison to data to Figure 3B.

Table 3. Gaussian Peak Parameters Used To Fit Valence-Band PES Data

PES feature	fit peak	binding energy (eV)	full width at half-maximum (eV)
A	1	11.0	2.0
	2	10.1	1.7
B	3	6.1	1.4
C	4	4.3	1.6
D	5	3.2	0.9
	6	2.6	0.9
	7	1.8	0.8
E	8	1.2	0.7
	9	0.5	0.7

ways: without subtracting the secondary tail, after subtracting out an exponential fit to the extremes of the spectrum, and after subtracting a third-order polynomial fit to the background extremes. The integrated intensities of the major features (peaks A–E) were determined by summing the areas of the Gaussians used to fit each peak region. The results are shown in Figure 5, where the total intensity of each spectrum has been normalized to 1 to allow comparison of the synchrotron data to the XPS spectrum as well as to account for any errors in the photon flux normalization procedure and changes in electron escape depth with changing electron kinetic energies. The exponential background-subtracted analysis for the 32-eV spectrum is used in Figure 5.

The experimental results in Figure 5 should be compared to the relative theoretical atomic cross sections of Figure 3B. (Note the differences in the photon-energy scale when making this comparison.) The peak A photon-energy dependence is quite similar to the C 2s atomic cross section in Figure 3B; both display the trend of increasing relative intensity with increasing photon energy, with the exception of the 32-eV data. This result both confirms this assignment and demonstrates that atomic trends can be observed in the fits to the valence-band data of these compounds. Another notable trend is observed in peak D, which has a relative-intensity maximum in the 50–80-eV region that compares favorably to the theoretical trend expected for the Ti 3d cross section in Figure 3B. An intensity maximum delayed after the ionization threshold is characteristic of transition metal 3d photoemission, and this behavior shows that this feature contains a significant amount of Ti 3d character in the states that

(41) Shirley, D. A. *Phys. Rev. B* **1972**, *5*, 4709.

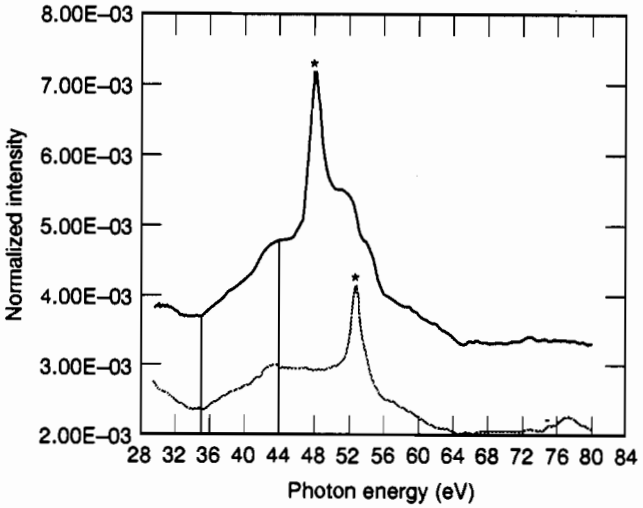

Figure 6. Partial-yield CFS spectrum for TiC(100) obtained with 10- (top) and 15-eV electrons. The large, sharp feature labeled with an asterisk is the result of the partial-yield window capturing the photoemission from the Ti 3p level. The onset of the absorption edge is near 35 eV and maximizes near 44 eV. These values should be compared to the Ti 3p binding energy in TiC (33.8 eV) and the ionization threshold of the Ti 3p levels (33.8 eV + work function), which is approximately 38 eV.

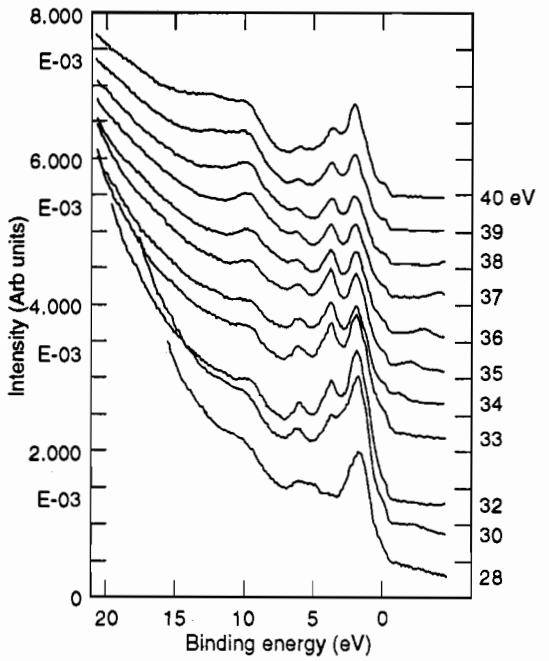

Figure 7. Valence-band PES data for TiC(100) obtained with photon energies below and at the Ti 3p absorption edge. A photoemission feature resulting from the excitation of the Ti 3p core level with second-order monochromator light is seen in the 34–37-eV data and also contributes to the lower energy data. Particularly note the shape of the 28-eV data, where the 2° peak contributes in the vicinity of peak B.

are producing these photoelectrons. The other three features do not show trends characteristic of any particular purely atomic cross section. Peaks B and C have a significant intensity drop when the photon energy is changed from 32 to 60 eV, strongly suggesting that they contain C 2p contributions. However, peaks B, C, and E all retain more intensity at 1486.6 eV than would be expected for pure C 2p levels, a result that indicates the existence of covalently mixed states in the valence-band spectrum. Possible contributors would appear to be the Ti 4s and 4p levels, each of which would have a relative increase in intensity when compared to the C 2p and Ti 3d levels when the photon energy approaches 1486.6 eV. This trend is also observed on the high-binding-energy side of the C 2s peak, an area that is more prominent in the 1486.6-eV data than at lower photon energies.

C. Resonant PES of TiC. The partial-yield CFS data obtained from TiC with two different kinetic-energy windows (centered at 10 and 15 eV) are presented in Figure 6. The onset of the Ti 3p absorption edge is evident near 35.5 eV in the CFS data, as are a change in slope near 39 eV and a relative maximum near 44 eV. These energies should be compared to the Ti 3p binding energy of 33.8 eV relative to the Fermi level (E_F) in TiC, indicating edge transitions to states just above E_F at the edge threshold. The sharp feature labeled with an asterisk in both CFS scans is the result of direct photoemission from the Ti 3p core levels, as shown by its 5-eV shift in the two data sets. The Ti 3s core level is also evident, especially in the KE = 15 eV spectrum (bottom) near 78 eV. These data show that the Ti 3s and 3p levels are separated by 25 eV, which was confirmed with the measured core level binding-energy difference of 25.1 eV. This implies that the onset of the Ti 3s absorption edge should be between 60 and 61 eV, although there are no distinct features in this energy region of the CFS scans to indicate 3s → unoccupied conduction band (antibonding levels) transitions.

Figure 7 provides valence-band data obtained over the range 28–40 eV, where significant changes in spectral intensity occur. One spectral feature that must be explained is the peak observed above the Fermi edge in the 34–37-eV data that moves to lower binding energy with increasing photon energy. This peak is the Ti 3p core level excited by second-order radiation from the monochromator, and it influences the shape of the valence band in the 28–33-eV data. Its effect is particularly evident in the 28-eV data, where the spectral shape is obviously different from that of the other data. The contributions of this second-order peak to the valence band must be considered in these data, but this peak also provides a convenient reference to indicate when the first-order photon energy is sufficient to excite Ti 3p electrons to states above E_F (approximately 34 eV). The utility of the second-order induced peak becomes evident when the relative kinetic energies of the electrons in this feature and those at the Fermi edge are compared. By definition, electrons at E_F (with a binding energy of 0) have a kinetic energy of KE = $h\nu - \phi$, where ϕ is the work function of the system. The core levels excited by the second-order radiation have a kinetic energy of KE = $2h\nu - BE - \phi$, where BE is the binding energy of the core level, 33.8 eV for the Ti 3p. The position of the second-order peak relative to E_F is simply the difference between these two energies, or $h\nu - BE$. Therefore, when the photon energy is exactly the binding energy of the core level, the second-order feature should appear exactly at E_F in the valence-band spectrum.

The most striking change in the valence-band-related peaks observed in the 28–40-eV photon range is the large reduction in intensity of the largest valence-band feature (peak D) at 34 eV, near the onset of the absorption edge. This peak starts to regain some of its lost intensity near photon energies of 39–40 eV. Significant intensity modulation in this photon energy range also occurs in the 6–12-eV binding-energy region, between the C 2s feature (peak A) and valence peak B. The data show an enhancement near the C 2s peak and an apparent decrease in the peak B intensity, although the background between the two features is also changing drastically as the photon energy is changed, likely indicating photoemission from states excited only at resonant-photon energies. These changes will be documented more carefully with fits to the spctra detailed below. Another change in the spectrum becomes evident in the 39- and 40-eV data in Figure 7, where a peak grows on the high-binding-energy side of the C 2s peak. The behavior of this region and remainder of the valence band is followed further in Figure 8.

The TiC valence-band spectrum is followed through the 40–60-eV photon energy range in Figure 8. The peak on the high-binding-energy side of the C 2s region observed at 40 eV grows in intensity and shifts to higher binding energy (staying at constant kinetic energy) as the photon energy is increased from 40 to 50

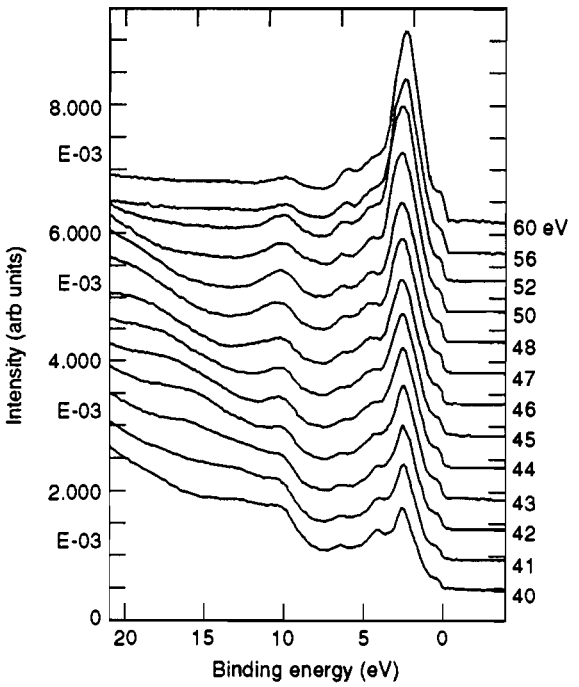

Figure 8. Valence-band spectra of TiC obtained over the photon-energy range of 40–60 eV. This is typically the photon-energy range in which resonant enhancement of Ti 3d features has been observed in other materials. Note the movement of the Ti MVV Auger feature to higher binding energy (remaining at constant kinetic energy).

eV, eventually shifting out of the spectral window. This peak is the Ti $M_{2,3}VV$ Auger peak with its intensity maximum having a kinetic energy of approximately 23.1 eV. However, the C 2s region retains its enhancement through 53 eV, even after the Auger peak has shifted out of this region. The remainder of the valence region also undergoes changes in Figure 8. In particular, peak D grows in intensity relative to the remainder of the valence band from 40 through 60 eV. Peak E also seems to be growing in this energy range while the changes in peaks B and C are subtle.

Valence-band spectral changes for the data in Figure 7 and 8 were quantified by fits as described in the previous section. The changes occurring in the C 2s region made the background particularly difficult to handle for these data. The fits over the 28–50-eV photon-energy range were conducted in two ways after subtracting out the exponential contributions from the secondary tail. In one group of fits, the C 2s region was ignored, and the Shirley background was constructed only for peaks B–E. The valence-band region was then fit with seven peaks (peaks 3–9 in Table 3), excluding the C 2s peaks. The second fitting procedure included the C 2s region (and the emerging Auger peak) in the Shirley background, and the data fits were conducted with the nine Gaussians described above, plus one Gaussian to account for the Auger intensity and another to account for changes in background intensity between the C 2s peak and peak B. The results of the data fits are presented in Figures 9 and 10, where the intensities of the seven main valence-band Gaussians are followed with photon energy for both of the fitting procedures. The intensity of the C 2s region is not plotted because background changes and the intrusion of the Auger feature hinder the analysis. However, it is clear that this region has an intensity maximum near 37–38 eV. The intensity plots in Figures 9 and 10 are grouped according to binding energy, with Gaussians 3 and 4 (peaks B and C), Gaussians 5–7 (peak D), and Gaussians 8 and 9 (part of peak D and peak E) shown on separate graphs.

The intensity plots in Figures 9 and 10 show differences in absolute intensities for the various peaks due to the different background-handling procedures, but the trends of intensity changes are generally consistent between the two methods. The

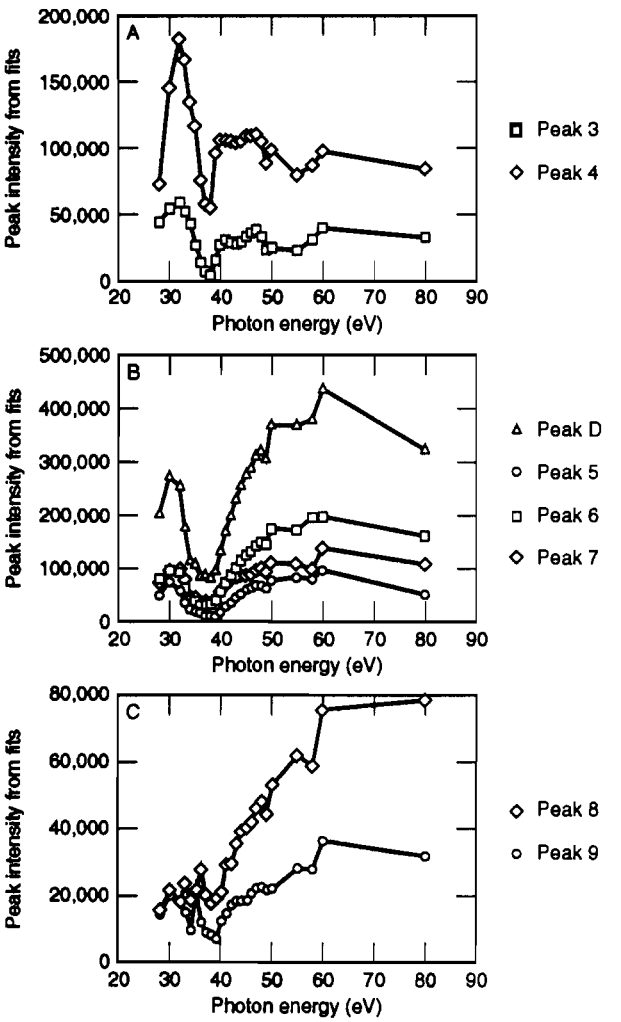

Figure 9. Integrated areas of the Gaussian peaks used to fit the spectral data from Figures 7 and 8: (A) intensity profiles of the high-binding-energy peaks 3 and 4; (B) intensity profiles of peaks 5–7 along with their sum (peak D); (C) intensity profiles of peaks 8 and 9 at low binding energy. These fits were generated after subtracting an exponential fit to the background extremes and using a Shirley background from 0 eV to the high-binding-energy side of peak B.

Figure 9 data show the intensity plots determined without the C 2s region included. In Figure 9A, peaks B and C (Gaussians 3 and 4) show a dramatic intensity decrease at the Ti 3p edge, followed by a rapid rise near 40 eV before leveling off. Figure 10A shows that the depth of this intensity minimum has been greatly exaggerated in the Figure 9A plot due to the inadequate handling of the background. In fact, for the Figure 9 fits, the peak width of Gaussians 3 and 4 had to be decreased to less than 0.8 and 1.3 eV, respectively, to fit the 37- and 38-eV data as compared to the nominal 1.4- and 1.7-eV widths used for these features in other fits. This indicates that only portions of the true peaks B and C valence features were being observed in these spectra, with much of the peaks obscured by increased background photoemission from other resonantly enhanced final states at higher binding energies. Valence-band features B and C, therefore, probably show only a modest intensity decline at the onset of the Ti 3p edge, followed by an intensity gain back to levels lower than pre-edge intensities, but intensities that might be expected on the basis of C 2p cross-section changes over this photon energy range.

The behavior of Gaussians 5–7 is displayed in the intensity plots of Figures 9B and 10B. In both figures, all of these features show a large intensity drop in the 34–40-eV region, followed by increases to levels somewhat above pre-edge intensities. The intensity of the PES feature peak D (followed at the sum of

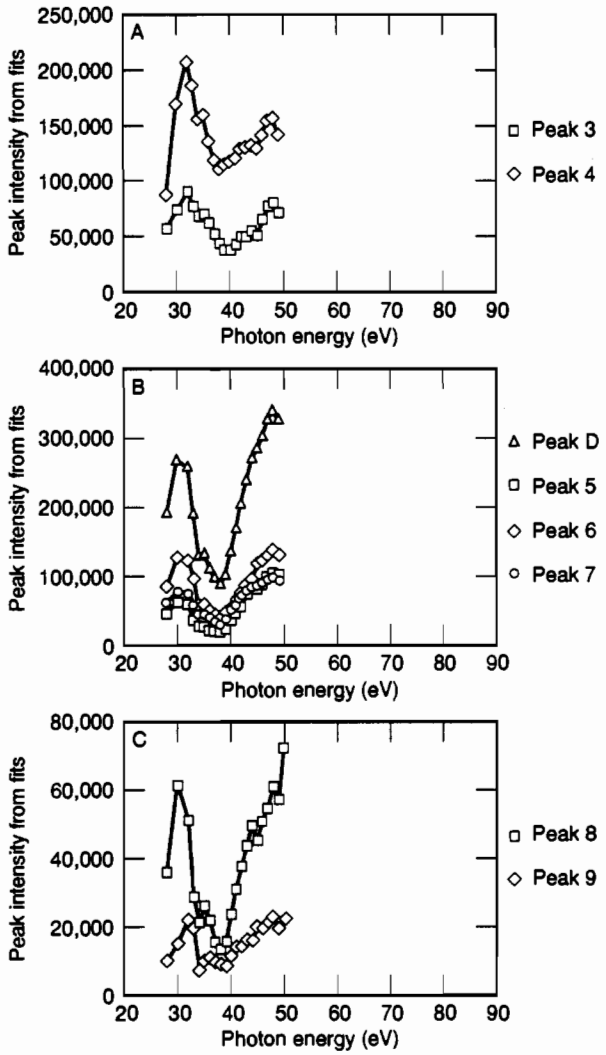

Figure 10. Intensity plots of the same fit peaks in Figure 9 determined with an exponential background and a Shirley background including the C 2s region.

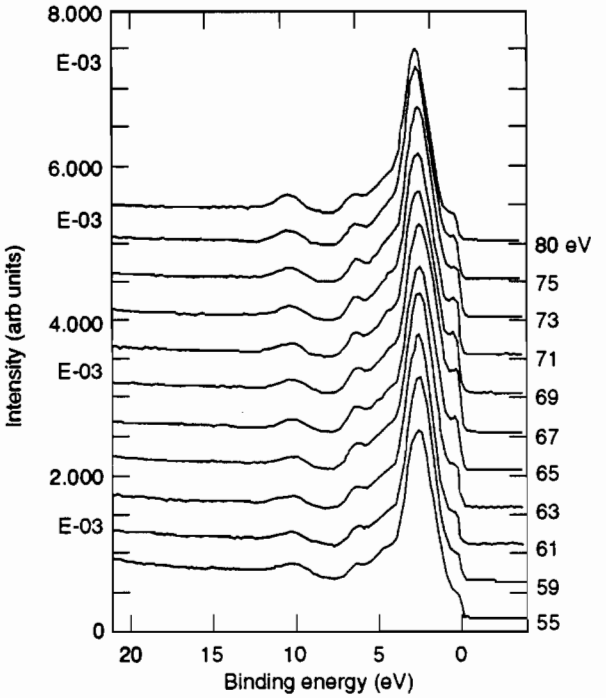

Figure 11. Valence-band spectra of TiC taken over the photon-energy range of 55–80 eV.

Gaussians 5–7 in Figures 9 and 10) shows this trend as well, with a greater than 50% intensity drop at the onset of the Ti 3p edge, followed by a modest intensity gain (roughly 40% relative to pre-edge intensity) in the 47–50-eV energy range. The nearly 3× intensity gain at 47 eV relative to the intensity minimum at 38 eV is different from the typical resonant enhancement of metal 3d features, which is often 2–3 times greater than *preresonance* intensities. This will be clearly demonstrated by the TiN results discussed below. Peak D shows further small intensity gains at higher photon energies, which may be due to other factors (cross section, escape depth, etc.). The results of the fits are consistent with the observed behavior in the spectra of Figures 7 and 8.

The intensity changes in the low-binding-energy region of the TiC valence band were followed with Gaussians 8 and 9. Gaussian 8 was predominantly in the low-binding-energy region of peak D, tailing into peak E, while Gaussian 9 was exclusively in the peak E region. These results are shown in Figures 9C and 10C. The peak 9 behavior is consistent between the two plots, showing an intensity decrease in the 35–40-eV region, followed by an intensity increase near 40 eV and a gradual rise at higher photon energies, which suggest the presence of some Ti character. Alternatively, the behavior of peak 8 was highly dependent on the background used. Without inclusion of the C 2s region, peak 8 behavior tended to mirror that of peak 9, indicating that it was contributing more to the lower binding-energy peak E than to peak D. In the Figure 10 plot, however, the behavior of peak 8 is much more reminiscent of peaks 5–7, displaying a large intensity decrease followed by a rise to pre-edge values. This changing behavior is an artifact of the fitting procedures and represents a difficulty in determining the resonant behavior of this spectral region. As with the entire valence-band region, there are no large resonance enhancements in the low-binding-energy region that would identify the existence of states having dominantly titanium 3d character.

D. Ti 3s Resonance? Further interesting changes occur in the TiC valence band in the 60–75-eV photon-energy region as demonstrated in Figure 11. The most striking change in the valence band occurring in this photon-energy region is the significant intensity increase of the lowest binding-energy feature (peak E), which goes through an intensity maximum near 67–68 eV. This effect and the other spectral changes occurring in these data are plotted in Figure 12, as determined by the same fitting procedures discussed earlier. Figure 12C documents the changes in the low-binding-energy (peak E) region. This graph presents the intensity profile of peaks 8 and 9 along with their sum plotted as peak E. Both peaks 8 and 9 (and hence their sum) show a distinct intensity increase in this photon-energy region. Consistent with the data in Figure 11, the total intensity peaks near 68 eV, although the lower energy peak 9 seems to maximize later than peak 8, which has a more rapid increase in the 62–65-eV region. The total range of intensity enhancement approximately spans the 60–76-eV region. Returning to the CFS absorption edge data of Figure 6, there are no edge features evident in this photon-energy range. However, this would be the energy range expected for the Ti 3s excitations to unoccupied conduction-band states (approximately 25 eV above the Ti 3p threshold). The sum of the peak 8 and 9 profiles shows that the intensity of the peak E region has been enhanced by a factor of about 2.5 relative to preresonance intensities, with peaks 8 and 9 having nearly the same enhancement.

The intensity changes for the remainder of the valence band are demonstrated in Figure 12A,B. In Figure 12B, the changes occurring for the peak D region are shown, both as broken down into the three Gaussian peaks (5–7) and as their sum. It is clear that the peak D region is not enhanced over this photon-energy range. Indeed, the region exhibits the gradual intensity decrease expected for most cross sections in this regime. In an examination of the individual components, some other interesting trends are

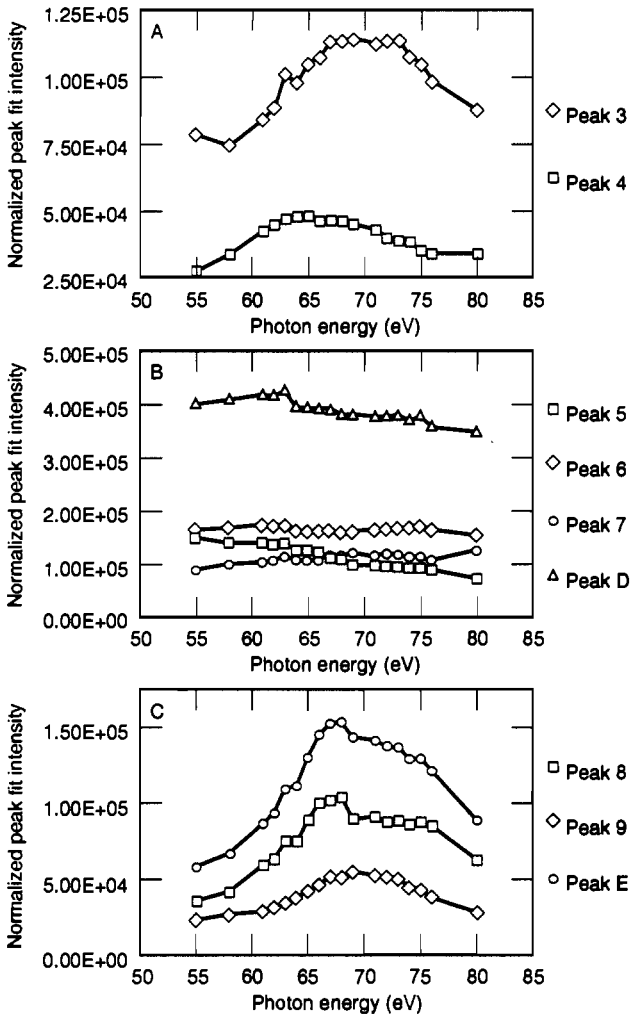

Figure 12. Intensity plots of the Gaussians used to fit the valence region of the spectra obtained from 55 to 80 eV: (A) plots of peaks 3 and 4; (B) plots of peaks 5–7 along with their sum (peak D); (C) plots of peaks 8 and 9 and their sum (peak E). The fits were obtained using Shirley backgrounds and are plotted according to binding energy.

evident. The largest contributor, peak 6, stays virtually constant through this energy range, perhaps exhibiting a small intensity dip in the 64–70-eV range. On the higher binding-energy side, peak 5 shows a definite decline over the entire photon-energy range. Alternatively, peak 7 on the low-binding-energy side actually displays an intensity increase over the range. (The increased intensity in the low-binding-energy region of peak D might be due to the presence of Ti 3d cross-section contributions.) This behavior creates the asymmetric shape of peak D that led to the requirement of fitting this region with three peaks. Overall, it is apparent that no enhancement of this region is taking place.

Figure 12A shows the changes occurring in the high-binding-energy peaks B and C (fit peaks 3 and 4). These plots clearly show that peaks 3 and 4 are enhanced over the 60–75-eV photon-energy range. The enhancement is not as great as observed in the low-binding-energy regions (factors of 1.4 for peak 3 and 1.5 for peak 4), but the shapes of the intensity profiles are quite similar to those of peaks 8 and 9. The possible assignments and implications of such a resonance will be addressed in detail in the Discussion.

E. Comparison to TiN Data. Valence-band data on TiN(110) were collected with fewer photon energies, although over the same energy range. Selected spectra are shown in Figure 13, with data spanning low and high photon energies. The overall shapes of the spectra are different from those observed for TiC, with generally less resolution, which might be attributable, to some degree, to the poorer quality of the sample. However, the

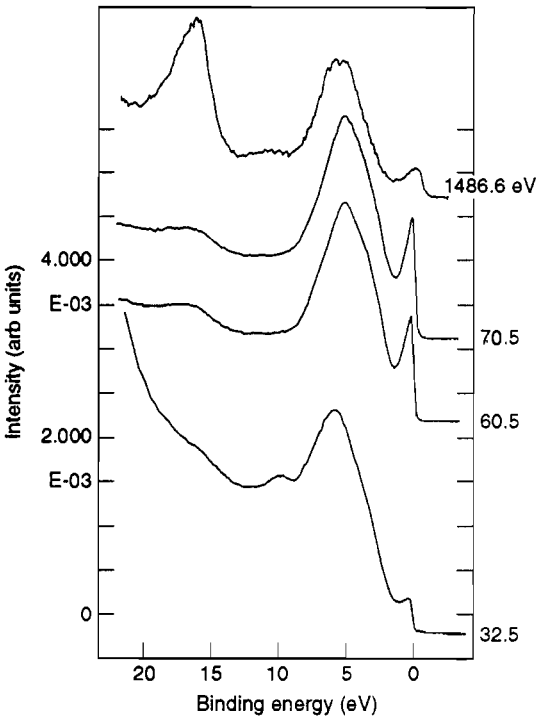

Figure 13. Valence-band PES data obtained from TiN(110) at the listed photon energies.

spectral shape is consistent with previously published data,[15] with the possible exception of the small feature near 9 eV, which is particularly prominent in the 32.5-eV data and could be due to surface impurities. The peak at the highest binding energy, near 17 eV, clearly exhibits behavior characteristic of the N 2s peak by analogy to the highest binding-energy peak of the TiC valence band. Specifically, this peak gains intensity relative to the remainder of the valence band with increasing photon energy and is the most intense feature at 1486.6 eV. A difference between TiN and TiC non-metal 2s regions is the more obvious presence of a high-binding-energy shoulder on the C 2s peak in the 1486.6-eV TiC data. The N 2s peak is asymmetric, but the asymmetry does not manifest itself as a well-defined feature, as with TiC. Additionally, the N 2s peak is narrower than the C 2s peak at 1486.6 eV because this high-binding-energy shoulder is either less intense or not split as far from the main peak, or both.

The most interesting feature in the remainder of the TiN valence band is the sharp peak near the Fermi level, separated from the rest of the valence band by approximately 2 eV. This peak goes through a relative intensity maximum between the low- and high-photon-energy data (≥70 eV), although insufficient data were taken to conclusively determine the precise location of this maximum. This behavior clearly defines this peak as containing significant Ti 3d character. The remainder of the TiN valence band is not as well resolved as the TiC data. However, the low-binding-energy portion of the main feature, at approximately 4 eV, is more prominent in the 60.5- and 70.5-eV data than at either extreme. Once again, this behavior is indicative of Ti 3d character, but the relative maximum is not as pronounced as in the dominant feature (peak D) for TiC. Overall, the well-defined higher binding-energy features clearly evident for TiC (peaks B and C) were not observed for TiN, and as with the N 2s peak, the main feature of the TiN valence band is somewhat narrower than that for TiC at 1486.6 eV. A general conclusion that can be drawn from this result is that the TiN valence levels are less perturbed by bonding interactions.

The TiN resonant behavior at the Ti 3p edge is shown in Figure 14, where both the CFS absorption-edge data and the valence-band spectra are displayed. The CFS scan shows the onset of the 3p transitions at 35.9 eV, slightly higher than seen for TiC. There

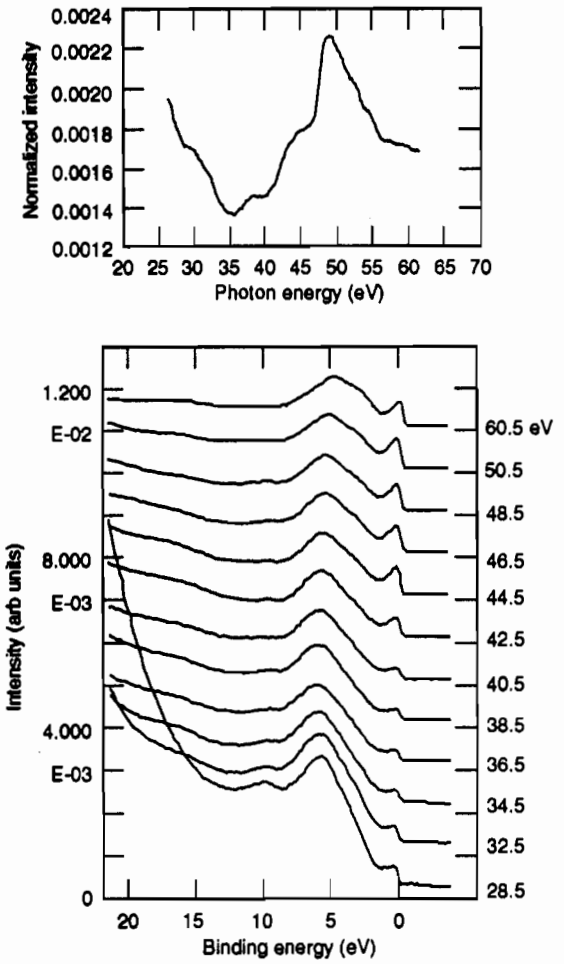

Figure 14. (A) Top: CFS data obtained from TiN with a kinetic-energy window centered at 10 eV. The large feature near 49 eV represents the Ti 3p photoemission peak. (B) Bottom: TiN valence-band data obtained with photon energies in the vicinity of the Ti 3p absorption edge.

Table 4. Gaussian Peak Parameters Used To Fit TiN Valence Data

peak	binding energy (eV)	width (eV)	peak	binding energy (eV)	width (eV)
1	9.9	2.5	4	4.0	2.7
2	6.8	2.6	5	0.90	1.0
3	5.6	1.7	6	0.45	0.4

is a small feature at 38.5 eV, followed by a more abrupt absorption starting at 41 eV and peaking near 44 eV. (The large feature at 49 eV is the Ti 3p PES peak, as discussed for TiC.) The valence-band spectra spanning the Ti 3p absorption region from 28.5 to 60.5 eV are presented in Figure 14B. The behavior of the lowest energy feature is the most notable change over this energy region. This peak shows an initial intensity drop starting at 32–33 eV, followed by an intensity enhancement at higher photon energies. An abrupt enhancement over the 40–44-eV range results in a peak that is much more intense than in preresonance data, more closely resembling the typical resonant effect observed for metal 3d features.[42]

The TiN data in Figure 14 were fit using procedures similar to those described earlier for the TiC data. The main valence features (excluding the N 2s) were fit with six Gaussians, one for the high-binding-energy feature, three in the large main band, and two for the sharp peak at low binding energy, as given in Table 4 and shown in Figure 15. The intensity profiles for these six peaks are provided in Figure 16; they are grouped together according to their binding-energy region. The profiles of peaks 5 and 6 (the low-binding-energy peak) were summed and are

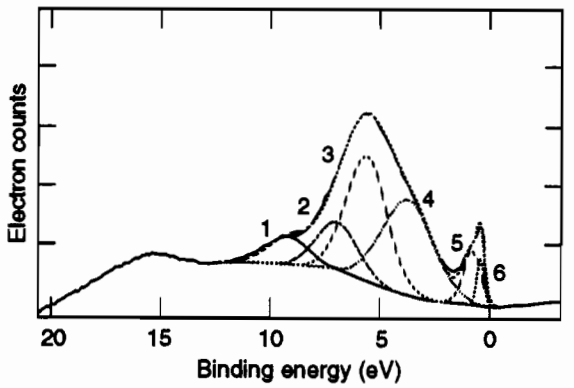

Figure 15. Fit of the 43-eV TiN valence-band spectrum using the six Gaussian peaks described in the text and in Table 4. An exponential fit to the secondary electron background has been subtracted from the data prior to fitting. The small feature near 17 eV is the N 2s peak.

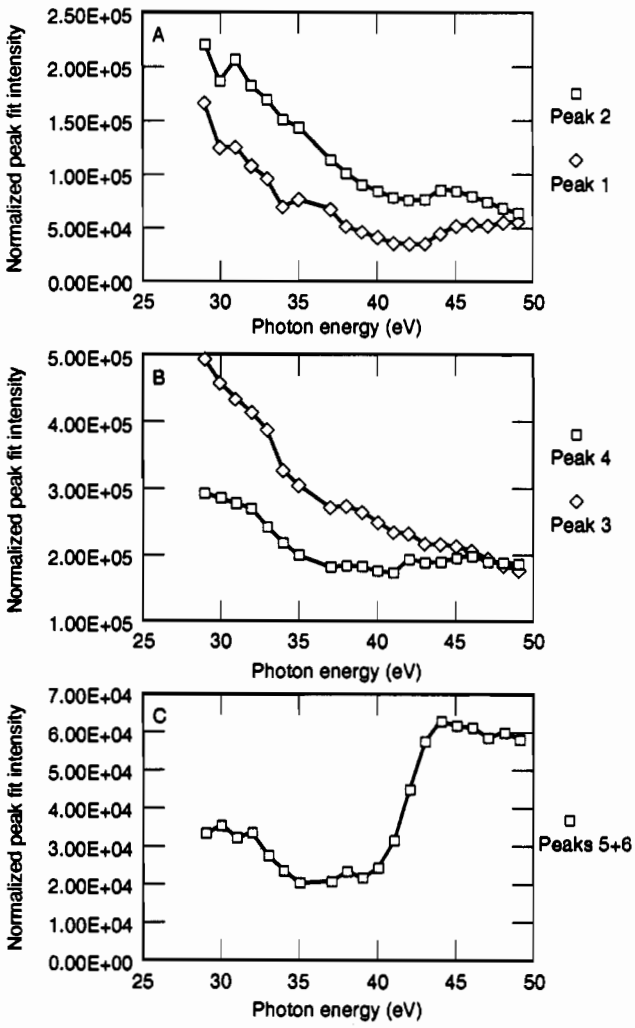

Figure 16. Intensity plots of the Gaussian peaks used to fit various portions of the TiN valence band near the Ti 3p resonance: (A) Gaussian peaks 1 and 2 from the high-binding-energy portion of the valence band; (B) Gaussian peaks 3 and 4 from the middle and lower binding-energy portions of the N 2p band; (C) sum of peaks 5 and 6 from the low-binding-energy peak.

presented in Figure 16C. These data (Figure 16C) show a typical Fano line shape for resonance interference effects, an initial dip followed by a large enhancement.[42,43] At the peak resonance maximum, this feature has been enhanced by a factor of approximately 2 relative to preresonance intensities. In addition, this profile displays a local intensity maximum at 38.5 eV, the

(42) Davis, L. C. *J. Appl. Phys.* **1986**, *59*, R25 and references therein.

(43) Fano, U. *Phys. Rev.* **1961**, *124*, 1866.

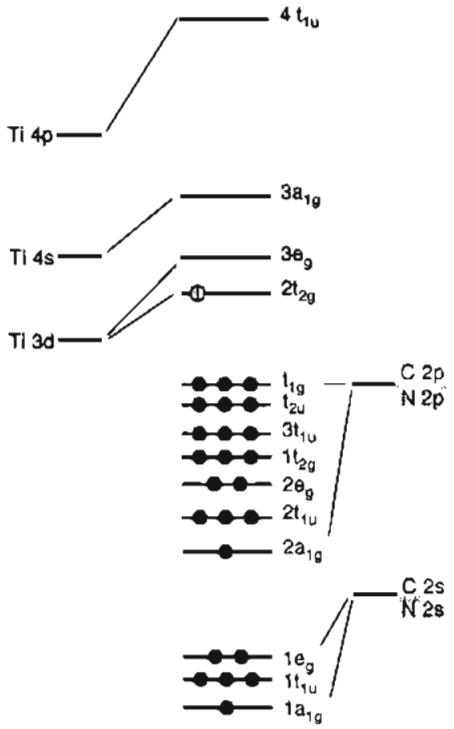

Figure 17. Qualitative molecular orbital diagram for TiC and TiN based on an octahedral TiX_6 complex. Each filled circle represents two electrons. The extra electron present in the TiN diagram is indicated by the lighter, half-filled circle in the $2t_{2g}$ level.

same energy as the feature in the CFS absorption edge. The intensity profile of this peak, therefore, follows the trends observed in the TiN absorption edge.

Other portions of the TiN valence band were not affected as greatly by resonance phenomena, as shown in Figure 16A,B. This is expected by analogy to the TiC valence band and confirms that these PES peaks were dominantly N 2p in character. Peaks 1 and 2 (high binding energy) in Figure 16A show some intensity modulation, each displaying a small intensity dip near 40–43 eV, followed by a slight intensity increase. Peaks 3 and 4 represent the mid- and low-binding-energy portions of the main N 2p band. Peak 3 shows very little modulation throughout this energy range, simply decreasing intensity, as expected for N 2p cross sections. Peak 4 displays a significant intensity dip at the edge, followed by a rise at energies corresponding to the large increase in the Ti d feature. This general trend for peak 4 is somewhat similar to that observed for peak D of TiC. However, the intensity changes in the TiN data are less evident than observed for TiC, likely reflecting the presence of lesser Ti d character in these dominantly N 2p levels than existed in the equivalent levels of TiC.

Discussion

The electronic structure of TiC and related materials (TiN, TiO) was first described using molecular orbital (MO) theory by Fischer to explain X-ray emission results.[44] Although several more complete treatments of the band structures of these materials have been performed since, the relatively straightforward MO diagrams provide an excellent foundation to understand the bonding in TiC and TiN.

An MO diagram for TiC and TiN is presented in Figure 17, modeled after those of Fischer and based on octahedral titanium-centered TiX_6 complexes. Since these materials have the same structure, the molecular orbitals should have the same relative ordering in both TiC and TiN, but the splittings should be different due to the differing amounts of covalent bonding between the atoms. For a TiC_6^{20-} cluster, all of the C 2p-based MOs are filled, but none of the Ti valence levels are occupied. This is consistent with the PES data discussed in this paper, as will be detailed below. Alternatively, the TiN_6^{15-} cluster has one additional electron, resulting in one electron in the Ti t_{2g} level. This picture is also consistent with the PES results that show a low-binding-energy peak separated from the remainder of the valence band (see Figure 13).

A more detailed examination of the TiC MO diagram actually shows very good agreement with the TiC valence-band data. Starting with the C 2s level, the diagram indicates that this feature should be split and that the higher binding-energy levels are formed through covalent-bonding interactions with the Ti 4s ($1a_{1g}$) and 4p ($1t_{1u}$) levels. This is supported by the asymmetric shape of the C 2s peak that is particularly evident in the 1486.6-eV spectrum. The relative cross-section contributions of the titanium 4s and 4p atomic levels should be at their greatest at this energy, making the asymmetry more obvious. This indicates that the C 2s levels are definitely involved in covalent-bonding interactions with Ti, despite the large energy difference in the atomic levels that would tend to limit this perturbation. The remaining portion of the C 2s peak should have e_g symmetry, according to the MO model, and can undergo σ-bonding with the Ti $3d_{z^2}$ and $d_{x^2-y^2}$ orbitals. The deepest binding energy levels present in the C 2p region (peaks B and C) are also formed through bonding interactions with the Ti 4s ($2a_{1g}$) and 4p ($2t_{1u}$) levels, and the PES results show a relative intensity increase at higher photon energies that confirms this assignment. The greater splitting of these levels from the remainder of the C 2p features, as compared to the 2s peak, shows that this bonding interaction is stronger for the 2p orbitals. This stronger interaction could be the result of the smaller energy difference between the atomic levels, greater overlap, or both.

The above discussion can also be applied to the results on TiN. However, the lack of well-defined peaks split from the main N 2s and 2p bands implies that the stabilization of these a_{1g} and t_{1u} levels through covalent-bonding interactions is not as great for TiN as that observed for TiC. This represents experimental evidence for greater covalent bonding in TiC. In addition, the low-binding-energy feature present in the TiN data but absent in the TiC data was clearly identified as containing dominantly Ti 3d atomic character by variable photon energy and resonant PES, consistent with the single-electron occupation of the $2t_{2g}$ MO in the TiN diagram in Figure 17.

According to the MO model, the portion of the TiC and TiN valence bands not yet discussed (i.e., peaks D and E for TiC) should be composed of bonding orbitals formed through interactions of the non-metal 2p orbitals with Ti 3d levels ($2e_g$, $1t_{2g}$) and either weakly bonding or nonbonding [$3t_{1u}$ (π), t_{2u}, t_{1g}] levels that should show little or no mixed cross-sectional behavior from covalent interactions. The variable photon-energy spectral data agree with this interpretation in a limited way. The predominant contributor to these PES features is certainly the non-metal 2p levels, as shown by the lack of strong resonant enhancement at the Ti 3p edge. In both TiC and TiN, there is evidence for some Ti 3d contribution in the low-binding-energy portion of the non-metal valence band (peak D for TiC, fit peak 4 for TiN), as discussed under Results and Analysis. In addition, it was apparent that the C 2p levels that did contain Ti d character displayed greater modulation from the Ti 3d cross-section contributions and resonance effects than did similar regions of TiN, again consistent with greater covalent mixing for the carbide. However, for both TiC and TiN, the 3d-containing levels ($2e_g$ and $1t_{2g}$ in the MO diagram) should appear at deeper binding energy relative to the nonbonding levels, which is inconsistent with the experimental findings that showed metal character in the lowest binding-energy regions of the non-metal bands. An explanation for this result can be found in the realization that these materials are not TiX_6 complexes but rather TiX extended lattices. The non-metal

(44) Fischer, D. W. *J. Appl. Phys.* **1970**, *41*, 3561.

atom is also surrounded by an octahedral array of titanium atoms, and one could conceivably generate an MO diagram for a CTi_6 complex quite readily. In such a diagram, the C 2p orbitals would transform as t_{1u} and, hence, could undergo strong σ-bonding interactions with group orbitals formed by the Ti 3d, 4s, and 4p levels. In this model, nonbonding C 2p orbitals would not exist, which is more in keeping with the experimental results. In reality, one should likely consider the electronic structure to be a hybrid of these two scenarios,[45] and molecular orbital calculations should be performed on high-symmetry, stoichiometric clusters to obtain accurate descriptions of their electronic structures.

The resonant PES data obtained on both TiC and TiN have provided some interesting results in general agreement with the MO description of electronic structure. The TiN results are a straightforward example of resonant PES at the Ti 3p edge. The Fano line shape of the low-binding-energy feature, with a 2× intensity enhancement that follows the absorption edge profile, demonstrates conclusively that this feature results from Ti 3d photoemission. The mechanism for this process that is consistent with the MO diagram and the formal oxidation state of Ti^{3+} is as follows:

$$\text{Ti } 3p^6 3d^1 \xrightarrow{h\nu} 3p^5 3d^2 \rightarrow 3p^6 3d^0 + e^- \qquad (1)$$

The resonance pathway proceeds via excitation of a Ti 3p core electron to an unoccupied Ti 3d MO, followed by an autoionization process similar to a super-Coster–Kronig (sCK) Auger decay. This mechanism has the same initial and final states as direct photoemission of the Ti 3d electron, resulting in the interference between the two pathways producing the Fano resonance profile. No other valence-band features of TiN exhibit a strong resonance that can be attributed to final states having predominantly Ti 3d character. The resonance effects on the N 2p valence-band features are restricted to the low-binding-energy region, which was also observed to contain contributions from Ti 3d levels through covalent-bonding interactions. Thus, with a molecular orbital constructed as a linear combination of atomic orbitals, one would expect resonance effects commensurate with the amount of covalent mixing in these states. The resonance profile observed for the low-binding-energy portion of the TiN N 2p band actually displays an effect often observed for ligand-based features at metal edges, an initial intensity decrease followed by a small enhancement. Bringans and Höchst[15] observed nearly identical resonance effects in stoichiometric TiN, with a significant enhancement of the low-binding-energy feature, a dip and small enhancement of the low-binding-energy portion of the N 2p band, and little effect on the remainder of the valence band. We believe that their description of the process, while correct in its intent, is described incorrectly with an initial electron configuration of Ti $3p^6 3d^2$. This electron configuration is inconsistent with the molecular orbital description for TiN that accurately predicts the valence-band shape in these materials.

The resonant effects on TiC are not as straightforward as those observed for TiN, a fact that is consistent with the lack of any occupied levels that are composed predominantly of Ti 3d orbitals. If such states existed, then we would have observed resonance profiles similar to those seen for the low-binding-energy peak of TiN and for other Ti materials that have well-characterized Ti 3d PES features, such as Ti_2O_3[46] and metallic titanium.[47] The lack of a strongly resonating valence-band peak for TiC indicates that the MO description of TiC with a formal Ti^{4+} ion provides an accurate electronic structure as opposed to an electron configuration that more closely resembles metallic or atomic titanium. The intensity modulation of the low-binding-energy portion of the C 2p band does indicate significant contributions from Ti 3d levels due to covalent mixing. The fact that greater enhancement of this region occurs for TiC again indicates greater mixing than observed for TiN.

The increase in photoemission in the 6–12-eV binding-energy region between the C 2p and C 2s bands is most likely due to the enhancement of shake-up final states at the Ti 3p edge. The mechanism for this enhancement would be as follows:

$$\begin{aligned}(\text{Ti } 3p^6)(\text{C } 2s^2)(\text{C } 2p^6)(\text{Ti } 3d^0) &\xrightarrow{h\nu} \\ (\text{Ti } 3p^5)(\text{C } 2s^2)(\text{C } 2p^6)(\text{Ti } 3d^1) &\rightarrow \\ (\text{Ti } 3p^6)(\text{C } 2s^2)(\text{C } 2p^4)(\text{Ti } 3d^1) + e^- \qquad (2)\end{aligned}$$

In this process, the electron excited to the unoccupied Ti 3d-based MO remains a spectator in the decay process that proceeds with the emission two electrons from the predominantly C 2p-based MOs. The final state resulting from this mechanism would have the equivalent energy of the photoemission of an electron from a C 2p-based MO plus the energy needed for a C 2p → Ti 3d charge transfer. In general, one would expect these states to appear on the high-binding-energy side of the C 2p MO PES peaks, and this is the region where significant background emission occurs in the 35–40-eV data. Optical reflection studies of TiC show numerous transitions in the 1–4-eV range, along with strong absorptions at 5.6 and 7.2 eV, most of which have been assigned as C 2p-based MO to Ti 3d-based MO transitions.[48] The shake-up structures observed with the Ti core levels in TiN appear at approximately 2.5 eV higher binding energy, while electron energy loss experiments place the ligand-to-metal charge-transfer transitions at 6.2 eV.[39] These experiments all show that shake-up states should appear at 1–7 eV higher binding energy compared to the main PES features in TiC. Another fact supporting the enhancement of shake-up features is the intensity loss in the main band (peaks B–E) TiC features in the 34–40-eV photon-energy range (Figures 9 and 10). This phenomenon is common for shake-up enhancement and is generally more pronounced in features that are related by symmetry to, and hence are covalently mixed with, the final states in which the excited electron remains following the decay process. In the current study, this implies that the valence-band features containing significant Ti 3d character should be influenced the most by this effect, as is observed for peak D. These results are similar to the enhancements observed at the S 2p edge of MoS_2, where shake-up final states on the high-binding-energy side of the S 3p-based valence-band features were observed.[49]

Our Ti 3p resonant PES results on TiC should be compared to those of Edamoto et al., who performed similar experiments on TiC(111) and TiC(100).[13] Their results on TiC(111) were significantly different from those on the (100) surface due to the presence of a surface state resulting from a Ti 3d-based state on the polar surface. This feature showed a distinct resonance, with its maximum near photon energies of 44 eV, and was clearly due to the emission of a Ti 3d electron. The authors use an electronic configuration similar to the Bringans and Höchst model used for TiN, with an initial-state configuration of Ti $3p^6 3d^2$, to represent the defect site. While such a configuration might be applicable to a defect, it clearly does not describe the configuration for stoichiometric (100), as demonstrated by both our variable photon-energy and resonance data. If such an initial state were present, then a strongly resonating valence-band feature should be observed on (100), which is not the case.

Edamoto et al. claim that the C 2s peak resonates on TiC-(111), with intensity increases noted at photon energies as low

(45) Didziulis, S. V.; Lince, J. R.; Fleischauer, P. D.; Yarmoff, J. A. *Inorg. Chem.* **1991**, *30*, 672.
(46) Smith, K. E.; Henrich, V. E. *Phys. Rev. B* **1988**, *38*, 9571.
(47) Bertel, E.; Stockbauer, R.; Madey, T. E. *Phys. Rev. B* **1983**, *27*, 1939.
(48) Alward, J. F.; Fong, C. Y.; El-Batanouny, M.; Wooten, F. *Phys. Rev. B* **1975**, *12*, 1105.
(49) Didziulis, S. V.; Lince, J. R.; Shuh, D. K.; Durbin, T. D.; Yarmoff, J. A. *J. Electron Spectrosc. Relat. Phenom.* **1992**, *60*, 175.

as 30 eV, well below the Ti 3p threshold. In addition, the intensity of the C 2s peak is greatly affected by the Ti $M_{23}VV$ Auger peak above the Ti 3p ionization threshold (particularly at 40 eV where their C 2s peak is at its maximum intensity). They acknowledge this overlap but do not quantify its influence. The authors also report that the C 2s region of the (100) surface is not influenced by resonant effects in this photon-energy region, with the only effect arising from the Ti Auger peak. Our results are clearly at odds with these findings since this spectral region is greatly influenced by resonant effects on the (100) surface, with intensity enhancements occurring at photon energies well below the ionization threshold. An interesting outgrowth of the MO description of the electronic structure and the strong Auger peak is the necessary participation of C 2p-based MOs in the sCK decay. The intensity of the Auger peak indicates that the shake-up states that are quite similar in nature to the Auger final states should also have high intensity. Edamoto et al. claim that the C 2s resonance can be explained by its similarity in symmetry to the surface state on the (111) surface and is not seen, therefore, on the (100) surface. We clearly disagree with this assertion because we see enhancement in this binding-energy region for TiC(100) and believe that shake-up states are the primary cause of intensity modulations observed for both of these surfaces. The intensity changes are not limited to the C 2s peak but occur over a wide binding-energy region. The possibility that the C 2s feature resonates cannot be disregarded in our data (perhaps due to significant covalent mixing with Ti 3d levels), but we feel that further theoretical analyses must be conducted to determine the nature and energy of shake-up features in TiC. Another interesting result in the resonant PES of TiC is that the shake-up states are enhanced at photon energies that correspond directly to the transition energies observed in the CFS data (35–40 eV), while resonant enhancement of Ti 3d-containing features generally displays a delayed resonance. This fact could indicate that these final states are not as strongly influenced by the relaxation phenomena that promote the delayed resonance and, hence, are not as strongly related to Ti 3d character as the main band PES features.

An interesting consequence of the good agreement between the MO description of bonding in TiC and the spectral data is the lack of any occupied states that are predominantly titanium based. This result precludes the possibility of any direct covalent bonds between titanium atoms that are not influenced by the carbon atoms in the lattice. The existence of any purely Ti–Ti bonding levels would have manifested itself in the data, particularly if d orbitals on neighboring atoms were participating in such a bond as has been proposed by Sundgren et al., for TiN.[50] This does not preclude overlap of d orbitals between titanium atoms but suggests that any such interaction is so strongly influenced by the neighboring C atoms that the resulting levels appear to be more like Ti–C bonding interactions. This interpretation argues for a highly delocalized bonding interaction among the atoms in TiC, and this likely contributes to the remarkable conductivity properties. Similar arguments can likely be made for TiN, as no levels with predominantly metal orbital character were observed to be stabilized to deeper binding in the TiN valence band. However, the presence of the Ti 3d peak at low binding energy makes the argument somewhat more ambiguous, and it is entirely possible that while the Ti 3d-based t_{2g} levels are antibonding with respect to Ti–N bonding, they could form σ-bonding orbitals between neighboring Ti atoms. This might explain the shorter metal–metal distance in, and greater conductivity of, TiN than is observed for TiC, while the greater Ti–C covalent bonding explains its higher hardness and melting point.

Another area worthy of discussion is the possibility of resonance phenomena observed in TiC at the Ti 3s absorption edge. To our knowledge, such a phenomenon has not been discussed in the literature, but we believe that a similar effect was observed by Bringans and Höchst in their work on TiN.[15] In that study, the intensity of the low-binding-energy region (0–2.1 eV) was enhanced relative to the remainder of the valence band (2.1–8.5 eV) in the 65–85-eV photon energy range, with the maximum occurring near 70 eV. This result is quite similar to the enhancement of the low-binding-energy region that we observed for TiC. There is one significant difference between TiC and TiN. In TiN, the lowest binding-energy feature is composed of Ti 3d-based states, while this feature is predominantly C 2p with Ti mixing in TiC. In examining the data treatment of Bringans and Höchst, one must recall that they took the integrated intensity between 0 and 2.1 eV and, hence, could have captured the low-binding-energy portion of the N 2p band that contains the analogous, low-binding-energy shoulder observed for TiC. Bringans and Höchst claimed that this effect was caused by a local minimum in the N 2p cross section, leading to an apparent increase in the intensity ratio at these photon energies. Our results clearly show an intensity increase in the TiC valence-band features in this photon-energy regime; the energy position of the Ti 3s absorption edge relative to this phenomenon must be considered to be more than coincidental. Further experimentation in this photon-energy regime on TiN with more careful attention paid to these phenomena would be of interest.

The possibility of resonance at the Ti 3s edge in TiC raises questions as to its mechanism. By analogy to resonance effects at the Ti 3p edge, the process must start with an excitation from this core level to an unoccupied state. Atomic-selection rules require that this final state have an $l = 1$ quantum number and most likely indicate a Ti 3s $\rightarrow$ 4p transition. Alternatively, in a strong octahedral field, the only transition allowed by symmetry from the A_{1g} initial state is to a T_{1u} final state, which can only be formed with the Ti 4p orbitals. Once again by analogy, the final states undergoing resonance enhancement would be required to contain significant Ti 4p character. However, our MO diagram and chemical common sense indicate that the Ti 4p level is unoccupied but that covalent mixing has created molecular orbitals with significant Ti 4p character. This would explain the resonance enhancement of the high-binding-energy C 2p features (particularly peak C) that we had assigned earlier as having t_{1u} symmetry. However, this still does not explain the nature of the low-binding-energy feature in TiC, which displays greater resonance enhancement than the high-binding-energy peaks. A partial explanation of this phenomenon may exist in the work of Hormandinger et al.,[51] who performed electronic structure calculations on TiO, the oxygen analog of TiC and TiN. These calculations included the Ti 4p levels and showed that there were more significant 4p contributions in the low-binding-energy regions of the oxide 2p band than in the deeper binding-energy feature. The nature of the Ti 3s resonance should be explored in more detail, with electronic structure calculations perhaps providing an explanation for the low-binding-energy feature that is not explicable through simple MO theory.

A final area to address is the differences in surface reactivity and tribological properties of the two materials on the basis of our understanding of their electronic structures. The presence of the lone electron in the antibonding t_{2g} level of TiN points to potentially greater surface reactivity for this material as compared to TiC. This electron resides very close to the Fermi level in TiN, and its relatively low binding energy and antibonding nature imply that its removal should be relatively facile and possibly favorable. Hence, one would expect TiN surfaces to be more readily oxidized than those of TiC. In addition, TiN surfaces are generally believed

(50) Sundgren, J.-E.; Johansson, B. O.; Rockett, A.; Barnett, S. A.; Greene, J. E. In *Physics and Chemistry of Protective Coatings*; Sproul, W. D., Greene, J. E., Thornton, J. A., Eds.; American Vacuum Society Series 2; American Institute of Physics: New York, 1986; pp 95–115.

(51) Hormandinger, G.; Redinger, J.; Weinberger, P.; Hobiger, G. Herzig, P. *Solid State Commun.* **1988**, *68*, 467.

to have higher coefficients of friction than those of TiC under similar conditions.[52] The potentially greater tendency of TiN to form surface bonds by donating electrons may provide a mechanism for greater friction of this material.

Conclusions

This study of the electronic structure of TiC and TiN has provided many important results to aid in understanding the chemical bonding in these materials. The PES data are well described by MO theory (particularly for TiC), proving the importance of covalent bonding between titanium and the non-metal atom. Furthermore, the participation of the Ti 4s and 4p levels in these covalent bonds was shown to be very important, making the inclusion of these interactions imperative in any theoretical examination of these materials. Many such calculations have ignored these bonding interactions. The resonant PES results at the Ti 3p edge have shown that no predominantly Ti 3d energy levels are occupied in TiC, indicating that purely Ti–Ti bonding interactions do not occur in TiC but they are possible in TiN. It has been postulated that the metallic electrical conductivity of these compounds necessitates the existence of direct Ti–Ti bonds, but this argument is not supported by the maximum in conductivity measured for stoichiometric TiN relative to samples that are deficient in nitrogen or contain excessive nitrogen.[50] In substoichiometric materials, the formation of Ti–Ti bonds should occur more readily due to a lesser influence of the non-metal atoms in the lattice resulting in greater conductivity (although one must consider the effect of lattice "defects" on conductivity). The possibility of Ti–Ti orbital overlap is not precluded by this finding, but the influence of the non-metal atom must be accounted for in any such interaction. It should be apparent that metal–metal bonds are not required for metallic conductivity; delocalization of electrons in conduction bands formed through covalent-bonding interactions between the metal and non-metal atoms should result in high conductivity. However, the possible Ti–Ti bonding in TiN could contribute to its greater conductivity relative to TiC.

(52) Roberts, E. W. European Space Tribology Laboratory, AEA Technology, U.K. Private communication.

The PES results also confirm that the fundamental relationship of the electronegativity difference between atoms does predict the extents of ionic and covalent interactions in these materials. The greater energy stabilization and greater mixed character of the bonding orbitals in TiC as compared to TiN are evidence for this trend. These factors likely contribute to the greater hardness and higher melting point of TiC relative to TiN (these trends continue for TiO as well), in addition to the extra electron occupying an antibonding level in TiN. It is also an interesting phenomenon that the extra electron or electrons provided by the N or O atom actually end up residing on the Ti atom, according to the MO description of electronic structure. This is entirely in keeping with the formal oxidation states of these materials.

The resonance phenomenon observed at the Ti 3s edge is intriguing and worthy of further study. It is possible that this effect is universal for transition metal compounds but that its presence has been masked due to material properties. Indeed, the high covalency of TiC may greatly contribute to the effect by mixing significant Ti 4p character into the valence band. It is clear that further experimental and theoretical examinations of these effects must be made before absolute conclusions of their origins can be made.

Acknowledgment. This work was funded by the Aerospace Sponsored Research program at the Aerospace Corp. and by Air Force Systems Command, Space and Missiles Command Contract No. F04701-88-C-0089. Research was conducted at the National Synchrotron Light Source (NSLS), Brookhaven National Laboratory, which is supported by the U.S Department of Energy, Division of Materials Sciences and Division of Chemical Sciences (DOE Contract No. DE-AC02-76CH00016). The authors thank S. Sakata of UBE Industries for the gift of the TiC single crystal, Dr. M. R. Hilton and M. B. Tueling (Aerospace) for growing the TiN thin film sample, Prof. K. D. Butcher of California Lutheran University for helpful discussions, and Dr. F. R. McFeely of IBM Yorktown Research Center and the staff at NSLC for their assistance.